Journal of Power Sources 209 (2012) 301–311

Contents lists available at SciVerse ScienceDirect

Journal of Power Sources

journal homepage: www.elsevier.com/locate/jpowsour

2D modeling of a flowing-electrolyte direct methanol fuel cell

C. Ozgur Colpan [a,*], Alan Fung [a], Feridun Hamdullahpur [b]

[a] Department of Mechanical and Industrial Engineering, Ryerson University, 350 Victoria Street, Toronto, Ontario, Canada M5B 2K3
[b] Mechanical and Mechatronics Engineering Department, University of Waterloo, 200 University Avenue West, Waterloo, Ontario, Canada N2L 3G1

ARTICLE INFO

Article history:
Received 11 October 2011
Received in revised form 29 February 2012
Accepted 1 March 2012
Available online 10 March 2012

Keywords:
Methanol
Direct methanol fuel cell
DMFC
Sulfuric acid
Flowing electrolyte
Modeling

ABSTRACT

A two-dimensional model of a flowing-electrolyte direct methanol fuel cell has been developed to predict the performance of the cell under various operating conditions. Governing equations including the proton and electron transport, continuity, momentum, species transport for methanol, water, and oxygen, and the auxiliary equations are coupled to determine the output parameters. These parameters are the concentration distribution of the species, cell voltage, power density, and the electrical efficiency of the cell. After validation with the experimental data, several simulations are carried out to study the effects of the fluid velocity at the fuel, air, and flowing electrolyte channel inlets on the output parameters. In addition, the effect of recirculating the methanol at the flowing electrolyte channel outlet is assessed. The results show that higher fluid velocities at the fuel, air, and flowing electrolyte channel inlets are needed to obtain higher power densities. However, an increase in the fluid velocity at the fuel channel inlet causes a decrease in the electrical efficiency of the cell. It is also found that the electrical efficiency of the FE-DMFC can be further increased if the methanol leaving the flowing electrolyte channel is recirculated into the methanol storage tank.

1. Introduction

Direct methanol fuel cell (DMFC) is one of the most promising technologies that can be used in portable power applications. This fuel cell is especially crucial for devices where high power density and long operation time are required, e.g. laptops and mobile phones [1]. The main distinctive feature of DMFC is its operation with liquid methanol. Some of the advantages of the liquid methanol are: easy to store, low cost, and high energy density. However, the cost of some of the components such as catalysts is still a major issue for its successful commercialization. In addition to its expensive components, main technical challenges with DMFC include the low power density and electrical efficiency due to the methanol crossover problem and the low rate of methanol oxidation kinetics on the anode [1,2].

There has been a significant progress in the DMFC research in last decade to overcome the technical issues mentioned above and to increase its performance. Controlling the operating parameters is one of the methods used in this regard. For example, the most well-known approach to minimize the effects of methanol crossover is to limit the methanol concentration at the fuel cartridge to levels such as 5 wt% [3]. Choosing appropriate materials for the components of the cell also plays an important role for the improvement of the performance. The common material for the membrane is Nafion®. This material is relatively durable and has high ionic conductivity and chemical stability; however it has high methanol and ruthenium crossover rate, high cost, low temperature limit, and high humidification [4]. Neburchilov et al. [4] reviewed alternative materials that can be used instead of Nafion® in a DMFC. They conclude that hydrocarbon and composite fluorinated membranes currently show the most potential for low cost membranes with low methanol permeability and high durability. Platinum–Ruthenium (Pt–Ru) is commonly used at the anode catalyst. As the usage of Pt increases the cost of the system significantly, Serov and Kwak [5] reviewed the non-platinum anode catalysts for DMFC applications. Their study showed that the performance of non-platinic catalysts is much lower than that of the platinum. However, new catalysts based on metal free carbon nitride nanotubes are promising support material for more active anode materials. Kamarudin et al. [6] discussed in their review paper that the combination of DMFC with thin film batteries (i.e. a hybrid power system) is one of the possible short-term solutions to overcome the economical issues associated with DMFC. In addition to controlling the operating parameters and the search in the alternative materials, new configurations and designs have been also proposed to increase the performance of the DMFC. Among them, one of the most promising designs is the Flowing-Electrolyte Direct Methanol Fuel Cell (FE-DMFC) [7], which is discussed below in detail.

The FE-DMFC, which was proposed by Kordesch et al. [7], is a novel DMFC design which provides performance improvement by eliminating the methanol crossover from the anode to the cathode.

* Corresponding author. Tel.: +1 416 979 5000; fax: +1 416 979 5265.
E-mail address: cocolpan@ryerson.ca (C.O. Colpan).

0378-7753/$ – see front matter © 2012 Elsevier B.V. All rights reserved.
doi:10.1016/j.jpowsour.2012.03.001

Nomenclature

ai_o	exchange current density times specific area ($A\,m^{-3}$)
C	concentration ($mol\,m^{-3}$)
D	coefficient of diffusion ($m^2\,s^{-1}$)
E^{Eq}	equilibrium voltage (V)
F	Faraday constant ($s\,A\,mol^{-1}$)
i	current density ($A\,m^{-2}$)
j	volumetric current density ($A\,m^{-3}$)
j_{xover}	crossover current density ($A\,m^{-3}$)
K_c	methanol oxidation reaction constant ($mol\,m^{-3}$)
l	length (m)
$\overline{LHV}$	lower heating value in molar basis ($J\,mol^{-1}$)
MW	molecular weight ($g\,mol^{-1}$)
n	normal vector
n_d	electro-osmotic drag coefficient
n_{repeat}	number of repeat elements
$\dot{N}''$	molar flow rate per cross section ($mol\,m^{-2}\,s^{-1}$)
P	pressure ($N\,m^{-2}$)
R	universal gas constant ($J\,K^{-1}\,mol^{-1}$)
S_c	source term in the conservation of species ($mol\,m^{-3}\,s^{-1}$)
S_u	source term in the momentum equation ($N\,m^{-3}$)
t	thickness (m)
T	temperature of the cell (K)
u	fluid velocity ($m\,s^{-1}$)
v	average fluid velocity ($m\,s^{-1}$)
V_{cell}	cell voltage (V)
$\dot{V}$	flow rate ($m^3\,s^{-1}$)
x	distance, m; molar ratio
y	distance (m)
w	width (m)
$\dot{W}''_{cell}$	power density of the cell ($W\,m^{-2}$)

Greek letters

α	transfer coefficient
ε	porosity
ρ	density ($g\,m^{-3}$)
σ	conductivity ($S\,m^{-1}$)
κ	permeability (m^2)
ξ	stoichiometric flow coefficient
μ	dynamic viscosity ($N\,m^{-2}\,s$)
η	overpotential (V)
η_{el}	electrical efficiency of the cell
ϕ	potential (V)
τ	shear stress ($N\,m^{-2}$)

Subscripts

a	anode
ac	air channel
c	cathode
eff	effective
fc	fuel channel
fec	flowing electrolyte channel
in	inlet
l	electrolyte phase
MeOH	methanol
s	electrode phase
xover	crossover

Superscripts

AC	air channel
FC	fuel channel
in	inlet
ref	reference

Schematics of a DMFC and a FE-DMFC are shown in Figs. 1 and 2, respectively. As can be seen from these figures, the FE-DMFC requires additional layers such as an additional membrane to separate the flowing electrolyte from the catalyst layer and a flowing electrolyte channel in which the diluted sulfuric acid flows to carry away the crossover methanol. This design basically reduces the cathodic overpotential as it hinders the amount of methanol reaching the cathode catalyst layer. However, the ohmic losses increase due to the inclusion of the additional layers. Diluted sulfuric acid is generally considered as the fluid to be pumped through the flowing electrolyte channel since it has high proton conductivity to reduce these additional ohmic losses. In addition, the performance of the cell could be further increased if the methanol recovered from the outlet of the flowing electrolyte channel could be separated from the sulfuric acid and recirculated back to the fuel channel inlet. The application areas of the FE-DMFC are more limited compared to the DMFC due to the additional system components. Some examples of the areas that FE-DMFC could be used include backup power for recreational activities, golf cars, and forklifts.

Performance of DMFC and FE-DMFC can be estimated through modeling studies. There have been numerous papers published on DMFC modeling. Some of the recent papers have included the multi-dimensional effects to predict the distributions of the output parameters in space (e.g. [8–11]), the two-phase transport taking into account the effects of the gaseous CO_2, CH_3OH, and H_2O (e.g. [10–12]), and the detailed water transport phenomena considering the combined effects of the hydraulic permeation, electro-osmotic drag, and diffusion at the thin membranes (e.g. [13–15]). As opposed to the many efforts in DMFC modeling, there have been only a few papers published in FE-DMFC modeling. Kjeang et al. [16,17] studied the methanol crossover reduction in the flowing electrolyte channel with different operating parameters; however the results of their study were limited since they did

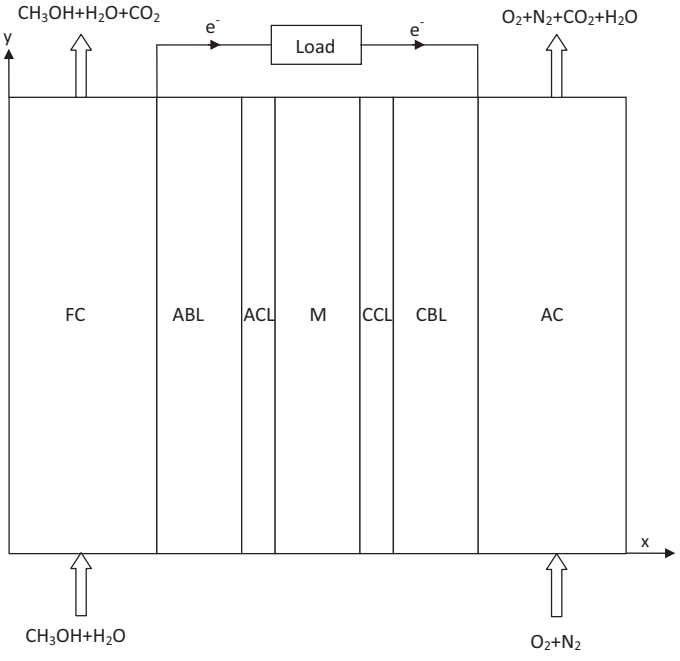

Fig. 1. Schematic of a 2D cross-section of the DMFC.

not include the transport phenomena in the backing layers as well as the fuel and air channels. In a recent publication, Colpan et al. [18] developed a one-dimensional FE-DMFC model to study the effects of flowing electrolyte channel thickness, concentration of methanol at the inlet, volumetric flow rate of the flowing electrolyte, and the recirculation of the methanol at the flowing electrolyte channel outlet. Their study showed that the maximum power densities of the DMFC and FE-DMFC are almost same; but the electrical efficiency of the recirculated FE-DMFC could be 57% more than that of the DMFC. In another publication, Ouellette et al. [19] developed an one-dimensional two-phase model to predict the effects of CO_2 formation on the performance of the FE-DMFC. Their study showed that the presence of CO_2 results in a reduction in the methanol crossover as well as the active area of the fuel cell.

The literature survey discussed above revealed that there has not been a paper published on the multi-dimensional model of a FE-DMFC, which takes into account the transport phenomena in all the layers of the cell. In this study, a two-dimensional model of a FE-DMFC has been developed to study the effects of the fluid velocity at the fuel, air, and flowing electrolyte channel inlets.

2. Modeling

A two-dimensional model of a FE-DMFC has been developed. For validation purpose, we have also developed a two-dimensional DMFC model using similar modeling approach and equations as the FE-DMFC. The details of the modeling for the FE-DMFC are presented in the following sub-sections. The main assumptions used in the modeling are as follows.

- The changes of the protonic and electronic conductivities within a layer are neglected.
- The formations of the CO_2 bubbles and water vapor are neglected; i.e. two phase effects are not taken into account.
- Membranes are fully hydrated.
- Methanol is fully consumed at the interface of the cathode membrane and the cathode catalyst layer.
- The effects due to the channel curvature are not taken into account.
- The flow in the electrolyte channel is considered as fully developed laminar flow.
- The fuel cell is isothermal.
- The fuel cell operates at the steady state condition.

2.1. Proton and electron transport equations

A liquid mixture consisting of methanol and water is pumped to the fuel cell through the fuel channel (FC). Some amount of these species diffuses through the anode backing layer (ABL), which is typically carbon cloth; and then they reach the anode catalyst layer (ACL) having Pt and Ru, where the protons and electrons are generated. The reaction occurring at the ACL is shown in Eq. (1).

$$CH_3OH + H_2O \rightarrow CO_2 + 6H^+ + 6e^- \quad (1)$$

The protons generated in the ACL reach the cathode catalyst layer (CCL) having Pt after they transport through Nafion® anode and cathode membranes (AM and CM) and flowing electrolyte channel (FEC) consisting of diluted sulfuric acid solution (i.e. H_2SO_4 and H_2O). The electrons are conducted to the external load through the ABL and the anode interconnect. These electrons reach the CCL after they pass through the cathode interconnect and the cathode backing layer (CBL). Please note that the interconnects are not taken into account in this study due to their high electronic conductivities. As the electrons and protons reach the CCL, they react with oxygen pumped to the cell through the air channel (AC) and transported through the CBL. The electrochemical reaction occurring at the CCL is shown in Eq. (2).

$$1.5O_2 + 6H^+ + 6e^- \rightarrow 3H_2O \quad (2)$$

The methanol crossing over the membranes and FEC, if any, also reaches the CCL. Here, the methanol reacts with oxygen as shown in Eq. (3).

$$CH_3OH + 1.5O_2 \rightarrow CO_2 + 2H_2O \quad (3)$$

According to the Ohm's law, the protonic and electronic current densities of the different layers can be shown as Eqs. (4) and (5), respectively. In these equations, l and s represent the electrolyte and electrode phases, respectively.

$$\boldsymbol{i_l} = -\sigma_l \nabla \phi_l \quad \text{(for ACL, AM, FEC, CM, and CCL)} \quad (4)$$

$$\boldsymbol{i_s} = -\sigma_s \nabla \phi_s \quad \text{(for ABL, ACL, CCL, and CBL)} \quad (5)$$

The charge balance for the electron conduction at the ABL and CBL is shown in Eq. (6); and the charge balance for the proton conduction at the AM, FEC, and CM is shown in Eq. (7). Here, it is assumed that there are no electron or proton losses in these layers.

$$\nabla \cdot \boldsymbol{i_s} = 0 \quad \text{(for ABL and CBL)} \quad (6)$$

$$\nabla \cdot \boldsymbol{i_l} = 0 \quad \text{(for AM, FEC, and CM)} \quad (7)$$

The charge balances for the proton and electron conduction at the ACL are shown in Eqs. (8) and (9), respectively. As the protons and electrons move in the opposite directions, the volumetric current density appears as a source term for the proton transport equation; whereas it is a sink term for the electron transport equation. The volumetric current density of the anode can be calculated using Eq. (10) [20]. The overpotential at the anode can be found using Eq. (11).

$$\nabla \cdot \boldsymbol{i_l} = j_a \quad (8)$$

$$\nabla \cdot \boldsymbol{i_s} = -j_a \quad (9)$$

$$j_a = \frac{a i_{oa}^{ref} C_{MeOH} \exp((\alpha_a F/RT)\eta_a)}{C_{MeOH} + K_c \exp((\alpha_a F/RT)\eta_a)} \quad (10)$$

$$\eta_a = \phi_s - \phi_l - E_a^{Eq} \quad (11)$$

The charge balances for the proton and electron conduction at the CCL are shown in Eqs. (12) and (13), respectively. Due to the chemical reaction of methanol with oxygen (Eq. (3)) occurring in this layer, the volumetric current density of the cathode decreases as shown in Eq. (14) due to a parasitic loss called as the crossover current density. The value of this current density can be calculated using the average molar flow rate of methanol reaching the interface of CM and CCL as shown in Eq. (15). The overpotential at the cathode is shown in Eq. (16).

$$\nabla \cdot \boldsymbol{i_l} = -j_c \quad (12)$$

$$\nabla \cdot \boldsymbol{i_s} = j_c \quad (13)$$

$$j_c + j_{xover} = a i_{oc}^{ref} \frac{C_{O_2}}{C_{O_2}^{ref}} \exp\left(\frac{-\alpha_c F}{RT}\eta_c\right) \quad (14)$$

$$j_{xover} = \frac{6F\dot{N}_{MeOH}^{''CM|CCL}}{t_{ccl}} \quad (15)$$

$$\eta_c = \phi_s - \phi_l - E_c^{Eq} \quad (16)$$

The boundary conditions applied to solve the electron and proton transport equations are shown in Eqs. (17)–(19). Eq. (19) shows the insulation boundary condition applied to the remaining boundaries; and k denotes both electrode and electrolyte phases.

$$\phi_{s,FC|ABL} = 0 \quad (17)$$

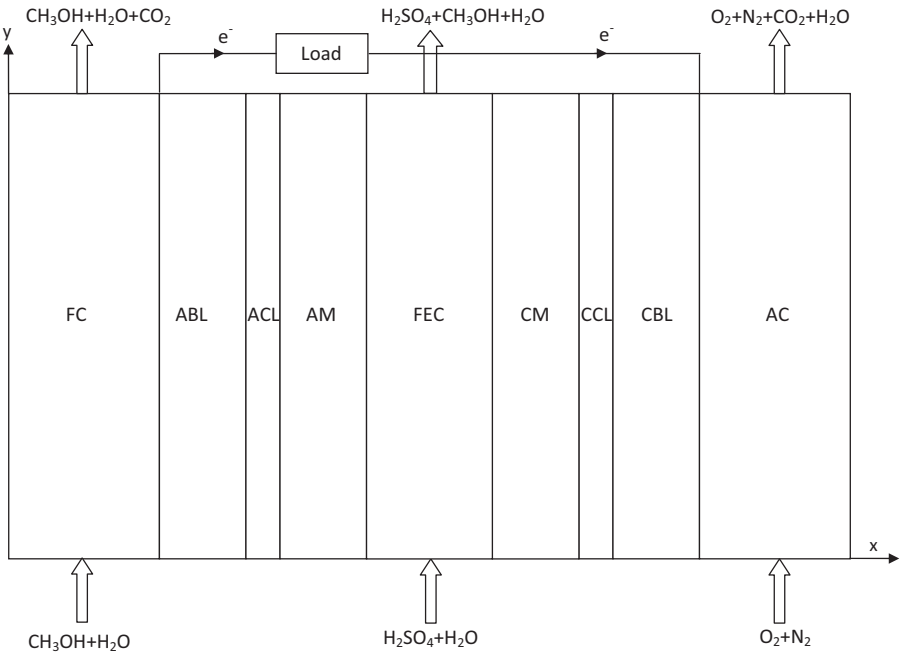

Fig. 2. Schematic of a 2D cross-section of the FE-DMFC.

$$\phi_{s,\mathrm{CBL|AC}} = V_{cell} \tag{18}$$

$$-\boldsymbol{n}\cdot\boldsymbol{i_k} = 0 \tag{19}$$

2.2. Continuity and momentum equations

The continuity equation for FC, ABL, CBL, and AC is shown in Eq. (20); and this equation for the catalyst layers is shown in Eq. (21). In the latter equation, k denotes any species, e.g. CH_3OH, H_2O, O_2, and CO_2, produced or consumed in a catalyst layer. For this layer, the gain or loss in the total mass of the fluid mixture originates from the production or consumption of the protons. The source or sink terms in the continuity equation of the catalyst layers can be calculated using the equations derived from the species transport equations as discussed in Section 2.3.

$$\rho\nabla\cdot\boldsymbol{u} = 0 \quad \text{(for FC, ABL, CBL, and AC)} \tag{20}$$

$$\rho\nabla\cdot\boldsymbol{u} = \sum S_{c,k}MW_k \quad \text{(for ACL and CCL)} \tag{21}$$

The momentum equation for FC, ABL, ACL, CCL, CBL, and AC can be given as Eq. (22) [20]. For the AC and FC, the porosity term is equal to 1. In this equation, the source term is zero for the AC and FC as shown in Eq. (23); whereas its value can be calculated using Darcy's law, Eq. (24), for the ABL, ACL, CCL, and CBL. For the AM and CM, the fluid velocity is assumed to be zero [20]. The velocity distribution in the FEC is found considering fully developed laminar flow conditions in this channel as shown in Eq. (26) [18].

$$\frac{\rho}{\varepsilon^2}(\boldsymbol{u}\cdot\nabla)\boldsymbol{u} = -\nabla P + \nabla\tau + S_u \quad \text{(for FC, ABL, ACL, CCL, CBL, and AC)} \tag{22}$$

$$S_u = 0 \quad \text{(for AC and FC)} \tag{23}$$

$$S_u = -\frac{\mu}{K}\boldsymbol{u} \quad \text{(for ABL, ACL, CCL, and CBL)} \tag{24}$$

$$\boldsymbol{u} = 0 \quad \text{(for AM and CM)} \tag{25}$$

$$u_y = \frac{6\dot{V}_{fec}(x - x_{\mathrm{AM|FEC}})(x_{\mathrm{FEC|CM}} - x)}{n_{repeat}w_{cell}t_{fec}^3} \quad \text{(for FEC)} \tag{26}$$

The average velocities at the fuel and air channel inlets are calculated using a reference condition and a stoichiometric flow coefficient as shown in Eqs. (27) and (28), respectively [20]. In these equations, width of the cell, w_{cell}, is equal to the summation of the widths of the channel and rib. For the walls, no-slip condition, Eq. (25), is applied.

$$v_{fc,in} = \frac{\xi_a i_{ref} l_{cell} w_{cell}}{6FC_{\mathrm{MeOH}}^{fc,in} t_{fc} w_{fc}} \tag{27}$$

$$v_{ac,in} = \frac{\xi_c i_{ref} l_{cell} w_{cell}}{4FC_{\mathrm{O_2}}^{ac,in} t_{ac} w_{ac}} \tag{28}$$

2.3. Species transport equations

2.3.1. Methanol transport

Methanol enters the fuel cell through the fuel channel. Due to the diffusion and convection mechanisms, some portion of it flows through the ABL and the remaining methanol exits through the fuel channel. The molar flow rate of methanol and the transport equation in the fuel channel are shown in Eqs. (29) and (30), respectively.

$$\dot{\boldsymbol{N}}'' = -D\nabla C + \boldsymbol{u}C \tag{29}$$

$$\nabla\cdot(-D\nabla C) + \boldsymbol{u}\cdot\nabla C = 0 \tag{30}$$

In the ABL, the diffusion and convection mechanisms are also effective in the transport of methanol to the ACL. However, an effective diffusion coefficient should be used considering the effects of porosity as shown in Eqs. (31)–(33).

$$\dot{\boldsymbol{N}}'' = -D_{\mathrm{eff}}\nabla C + \boldsymbol{u}C \tag{31}$$

$$\nabla\cdot(-D_{\mathrm{eff}}\nabla C) + \boldsymbol{u}\cdot\nabla C = 0 \tag{32}$$

where

$$D_{\mathrm{eff}} = \varepsilon^{1.5}D \tag{33}$$

In the ACL, the production of protons leads to the drag of methanol to the membrane due to the electro-osmosis effect. The molar flow rate of methanol and the transport equation at this layer

can be shown as Eqs. (34) and (35), respectively. Combining Eq. (35) and (8), the transport equation can be shown as Eq. (36).

$$\dot{\boldsymbol{N}}'' = -D_{\text{eff}}\nabla C + \boldsymbol{u}C + n_d^{\text{MeOH}}\frac{\boldsymbol{i_l}}{F} \tag{34}$$

$$\nabla\cdot(-D_{\text{eff}}\nabla C) + \boldsymbol{u}\cdot\nabla C + \frac{n_d^{\text{MeOH}}\nabla\cdot\boldsymbol{i_l}}{F} = \frac{-j_a}{6F} \tag{35}$$

$$\nabla\cdot(-D_{\text{eff}}\nabla C) + \boldsymbol{u}\cdot\nabla C = \frac{-j_a}{F}\left(\frac{1}{6} + n_d^{\text{MeOH}}\right) \tag{36}$$

In Eqs. (35) and (36), the drag coefficient of diluted methanol is considered as constant using the average concentrations of methanol and water at the interface of ACL and AM, which is shown in Eq. (37) [20].

$$n_d^{\text{MeOH}} \cong n_d^{\text{H}_2\text{O}}\left.\frac{C_{\text{MeOH}}}{C_{\text{H}_2\text{O}}}\right|_{\text{ACL|AM}} \tag{37}$$

In the AM and CM, the convective flow is neglected as mentioned in Section 2.2. Hence, electro-osmosis and diffusion are the only mechanisms considered as shown in Eqs. (38) and (39). Combining Eqs. (7) and (39), the transport equation reduces to Eq. (40).

$$\dot{\boldsymbol{N}}'' = -D_{\text{eff}}\nabla C + n_d^{\text{MeOH}}\frac{\boldsymbol{i_l}}{F} \tag{38}$$

$$\nabla\cdot(-D_{\text{eff}}\nabla C) + \frac{n_d^{\text{MeOH}}\nabla\cdot\boldsymbol{i_l}}{F} = 0 \tag{39}$$

$$\nabla\cdot(-D_{\text{eff}}\nabla C) = 0 \tag{40}$$

In the FEC, the effect of the convective flow of sulfuric acid solution should be taken into account. Using a similar approach with a previous study conducted by Colpan et al. [18], this effect has been considered as a sink term in the methanol transport equation. The molar flow rate of methanol is shown in Eq. (41). Using the velocity of the FEC shown in Eq. (26), the methanol transport equation at this layer can be shown as Eq. (42). Combining Eqs. (7) and (42), the methanol transport equation reduces to Eq. (43).

$$\dot{\boldsymbol{N}}'' = -D_{\text{eff}}\nabla C + n_d^{\text{MeOH}}\frac{\boldsymbol{i_l}}{F} \tag{41}$$

$$\nabla\cdot(-D_{\text{eff}}\nabla C) + \frac{n_d^{\text{MeOH}}\nabla\cdot\boldsymbol{i_l}}{F} = -\frac{6\dot{V}_{fec}C(x - x_{\text{AM|FEC}})(x_{\text{FEC|CM}} - x)}{n_{repeat}L_{cell}w_{cell}t_{fec}^3} \tag{42}$$

$$\nabla\cdot(-D_{\text{eff}}\nabla C) = -\frac{6\dot{V}_{fec}C(x - x_{\text{AM|FEC}})(x_{\text{FEC|CM}} - x)}{n_{repeat}L_{cell}w_{cell}t_{fec}^3} \tag{43}$$

2.3.2. Water transport

The main equations for water transport at the FC and ABL are similar with those for methanol transport given in Eqs. (29)–(33). For the ACL, diffusion, convection, and electro-osmosis affect the transport of water as shown in Eqs. (44) and (45). Combining Eqs. (8) and (45), the transport equation can be shown as Eq. (46). In this study, we assumed a constant concentration profile for water at the AM, FEC, and CM [18].

$$\dot{\boldsymbol{N}}'' = -D_{\text{eff}}\nabla C + \boldsymbol{u}C + n_d^{\text{H}_2\text{O}}\frac{\boldsymbol{i_l}}{F} \tag{44}$$

$$\nabla\cdot(-D_{\text{eff}}\nabla C) + \boldsymbol{u}\cdot\nabla C + \frac{n_d^{\text{H}_2\text{O}}\nabla\cdot\boldsymbol{i_l}}{F} = \frac{-j_a}{6F} \tag{45}$$

$$\nabla\cdot(-D_{\text{eff}}\nabla C) + \boldsymbol{u}\cdot\nabla C = \frac{-j_a}{F}\left(\frac{1}{6} + n_d^{\text{H}_2\text{O}}\right) \tag{46}$$

2.3.3. Oxygen transport

The main equations for the oxygen transport at the AC and CBL are similar to those for the methanol transport equations, Eqs. (29)–(33). In the CCL, the oxygen consumption due to the methanol crossover and the electrochemical reaction appear as a sink term. The molar flow rate and transport equation for oxygen at the CCL are shown in Eqs. (47) and (48), respectively.

$$\dot{\boldsymbol{N}}'' = -D_{\text{eff}}\nabla C + \boldsymbol{u}C \tag{47}$$

$$\nabla\cdot(-D_{\text{eff}}\nabla C) + \boldsymbol{u}\cdot\nabla C = \frac{-1}{4F}(j_c + j_{xover}) \tag{48}$$

2.3.4. Boundary conditions

The concentration of the methanol at the fuel channel inlet is known, Eq. (49); and the concentrations of the water at the fuel channel inlet and oxygen at the air channel inlet can be calculated from the given input data. As the fuel storage tank of the fuel cell system consists of water and methanol with a constant volume, the concentration of water at the fuel channel inlet can be given in terms of the concentration of methanol as shown in Eq. (50). The oxygen concentration at the inlet of the air channel can be expressed in terms of the molar ratio of oxygen in the air and inlet pressure of the air channel as shown in Eq. (51).

$$C_{\text{MeOH}}^{fc,in} = \text{Known} \tag{49}$$

$$C_{\text{H}_2\text{O}}^{fc,in} = \frac{\rho_{\text{H}_2\text{O}}}{MW_{\text{H}_2\text{O}}}\left(1 - \frac{C_{\text{MeOH}}^{fc,in}MW_{\text{MeOH}}}{\rho_{\text{MeOH}}}\right) \tag{50}$$

$$C_{\text{O}_2}^{ac,in} = x_{\text{O}_2}\frac{P_{ac,in}}{RT} \tag{51}$$

In this study, it is assumed that the entire methanol reaching the CCL is consumed at the interface of CM and CCL as shown in Eq. (52). It should be noted that if the flow rate of sulfuric acid is high enough, the concentration of methanol can become zero within the FEC or CM.

$$C_{\text{MeOH}}^{\text{CM|CCL}} = 0 \tag{52}$$

Continuity equations are used for all the interior boundaries. The outflow boundary condition, Eq. (53), for the channel outlets and no-flux boundary condition, Eq. (54), for the remaining boundaries are applied.

$$-\boldsymbol{n}\cdot\nabla C_k = 0 \tag{53}$$

$$-\boldsymbol{n}\cdot\dot{\boldsymbol{N}}_{\boldsymbol{k}}'' = 0 \tag{54}$$

2.4. Output parameters

The average current density of the cell can be calculated using Eq. (55).

$$i_{cell} = \frac{1}{l_{cell}}\iint_{\text{ACL}} j_a\,dx\,dy \tag{55}$$

The power density of the cell, and the electrical efficiency of the cell can be found using Eqs. (56) and (57), respectively.

$$\dot{W}_{cell}'' = i_{cell}V_{cell} \tag{56}$$

$$\eta_{el} = \frac{\dot{W}_{cell}''}{\dot{N}_{\text{MeOH}}''^{fc,in}\overline{LHV}} \tag{57}$$

If the flowing electrolyte is recirculated, the electrical efficiency can be shown as follows.

$$\eta_{el} = \frac{\dot{W}_{cell}''}{(\dot{N}_{\text{MeOH}}''^{fc,in} - \dot{N}_{\text{MeOH}}''^{fec,out})\overline{LHV}} \tag{58}$$

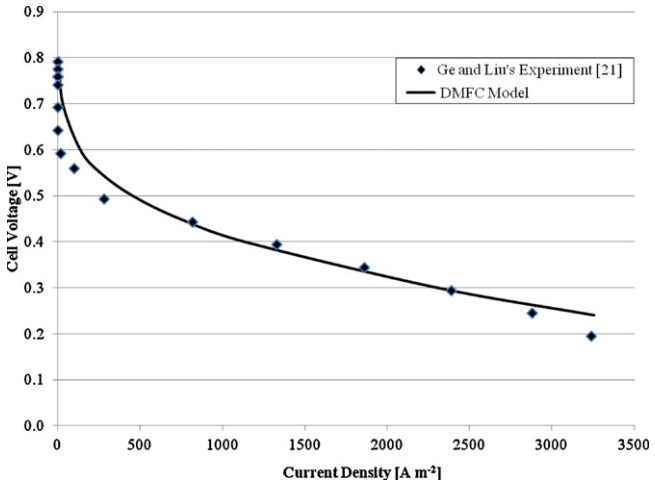

Fig. 3. Validation of the 2D DMFC model.

3. Results and discussion

The results and discussion for the validation of the model and the parametric studies including the effects of the fluid velocities at fuel, air, and flowing electrolyte channel inlets are presented in this section. The main input data used in the simulations are shown in Table 1. The solution of the set of the equations given in Section 2 is done using Comsol Multiphysics 4.2, which is software based on the finite element method. After a grid independent analysis, 51,817 triangular elements are taken for the geometry chosen.

3.1. Validation of the model

The results of the 2D DMFC model developed are compared to the experimental data published by Ge and Liu [21]. The geometrical dimensions of the cell and the main operating parameters are given in Table 1. In their experiments, the following materials were used as the components of the cell: Nafion® 117 for the membrane, carbon cloth for the anode and cathode backing layers, Pt–Ru with a loading 3 mg cm^{-2} for the anode catalyst layer, and Pt-black with a loading of 3 mg cm^{-2} for the cathode catalyst layer. The comparison of the experimental data and the results of the simulation of the model between the cell voltages of 0.2 V and 0.8 V is shown in Fig. 3. As can be seen from this figure, there is a good agreement between the experimental and modeling data. The minor discrepancy at the low current density conditions can be attributed to the simplified equations used for electrochemical relations, Eqs. (10) and (14), occurring at the anode and cathode catalyst layers. At high current densities such as 3000 A m^{-2}, the experimental results show a deviation from linearity due to the diffusion limitations; however as this deviation occurs at higher current densities (i.e. current densities higher than 3000 A m^{-2}) for the model developed, the modeling results show a linear trend for the high current density conditions shown in Fig. 3. The reason of this discrepancy at these conditions can be attributed to neglecting the two-phase effects in the model developed; which has a significant effect on the limiting current density.

3.2. Effect of the fluid velocity at the fuel channel inlet

The velocity of the diluted methanol solution at the fuel channel inlet can be represented by the stoichiometric flow coefficient as shown in Eq. (27). For the given coefficient, methanol concentration at the inlet, geometry of the cell, and chosen reference current density, which is taken as 1500 A m^{-2}, this velocity is first calculated. In the simulations, the volumetric flow rate of the sulfuric

Table 1
Input data for the base case.

Input parameter	Value
Length of the cell	6.5×10^{-2} m [8]
Width of the air and fuel channels	1×10^{-3} m [8]
Width of the repeat element	2×10^{-3} m [8]
Thickness of the air and fuel channels	8×10^{-4} m [8]
Thickness of the anode and cathode backing layers	1.4×10^{-4} m [8]
Thickness of the anode and cathode catalyst layers	3×10^{-5} m [8]
Thickness of the membrane (DMFC)	1.83×10^{-4} m [22]
Thickness of the anode and cathode membranes (FE-DMFC)	9.2×10^{-5} m [18]
Thickness of the flowing electrolyte channel	5×10^{-4} m [18]
Number of repeat elements in a single cell	32
Molar concentration of the methanol at the fuel channel inlet	2000 mol m^{-3}
Molar ratio of oxygen at the air channel inlet	21%
Stoichiometric flow coefficient at fuel channel inlet	2
Stoichiometric flow coefficient at air channel inlet	3
Volumetric flow rate of the flowing electrolyte per single cell	1.67×10^{-7} m^3 s^{-1}
Temperature of the cell	70 °C
Pressure of the anode and cathode outlets	1 atm
Porosity of the anode and cathode backing layers	0.6 [8]
Porosity of the anode and cathode catalyst layers	0.4 [8]
Porosity of the membranes	0.28 [8]
Porosity of the spacer in the flowing electrolyte channel	0.6 [18]
Permeability of the anode and cathode backing layers	2×10^{-12} m^2 [23]
Permeability of the anode and cathode catalyst layers	10^{-13} m^2 [23]
Permeability of the flowing electrolyte channel	2×10^{-12} m^2 (assumed)
Coefficient of diffusion of methanol in water	$2.8 \times 10^{-9} \times e^{[2436((1/353)-(1/T))]}$ m^2 s^{-1} [24]
Coefficient of diffusion of methanol in Nafion®	$4.9 \times 10^{-10} \times e^{[2436((1/333)-(1/T))]}$ m^2 s^{-1} [24]
Coefficient of diffusion of oxygen in gas	$\left(\frac{T^{1.75} \times 5.8 \times 10^{-8}}{27.772 \times P_c}\right)$ m^2 s^{-1} [25]
Electro-osmotic drag coefficient of water	$1.6767 + 0.0155 \times T + 8.9074 \times 10^{-5} \times T^2$ (T is in °C) [26]
Cell voltage	0.4 V
Protonic conductivity of the membrane	10 S m^{-1} [22]
Protonic conductivity of the sulfuric acid solution	145 S m^{-1} [18,27]
Electronic conductivity of the backing layers	300 S m^{-1} [28]
Methanol oxidation reaction constant	2.265×10^{-3} mol m^{-3} [29]
Reference oxygen concentration	0.472 mol m^{-3} [8]
Anodic transfer coefficient	0.5 [8]
Cathodic transfer coefficient	0.5 [8]
Reference exchange current density times specific area at anode	6×10^5 A m^{-3} (calibrated)
Reference exchange current density times specific area at cathode	200 A m^{-3} [8]
Reference current density for calculating the fluid velocity	1500 A m^{-2} [23]

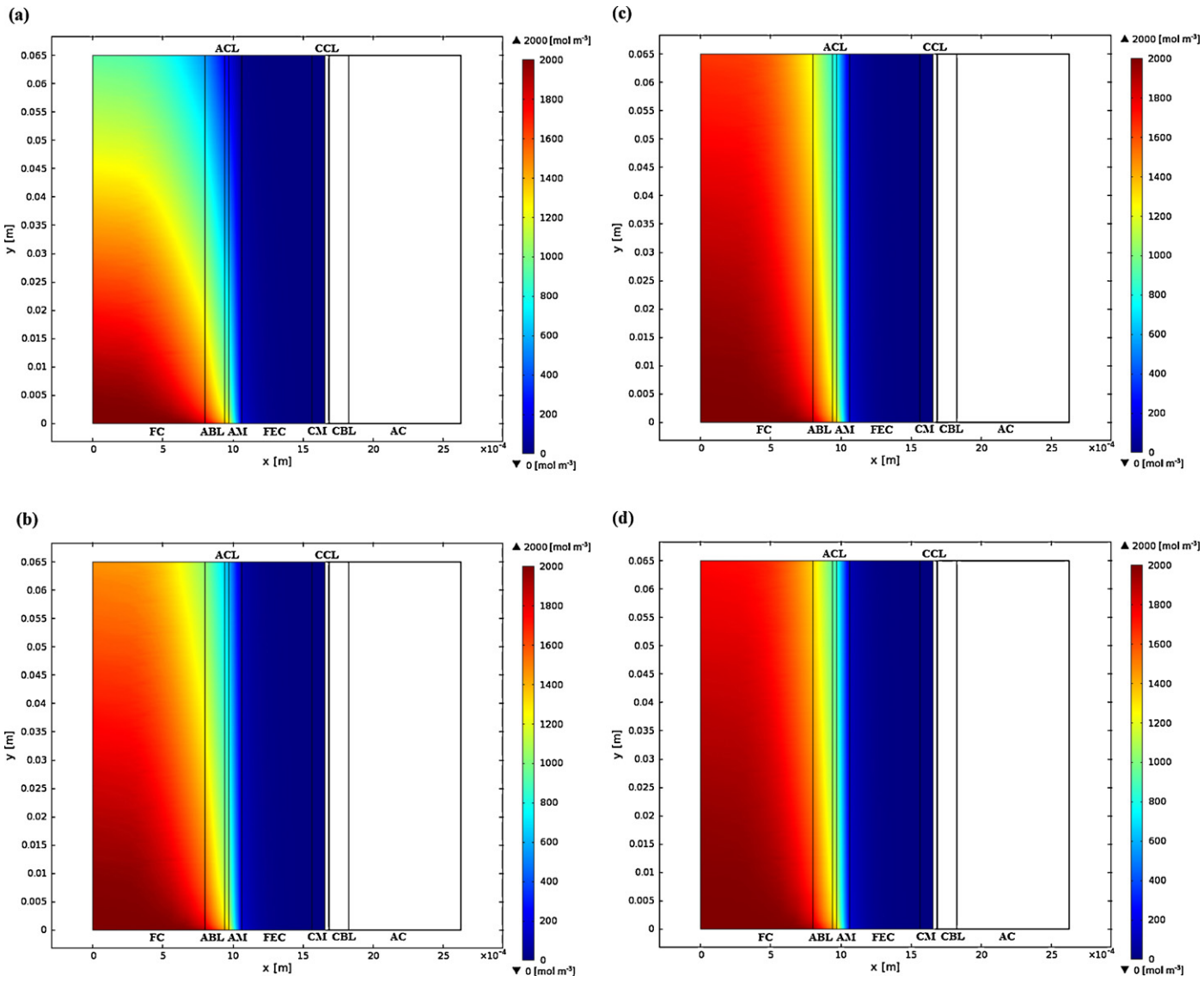

Fig. 4. Methanol concentration distribution of the FE-DMFC for different fuel channel inlet velocities: (a) $\xi_a = 1$ or $v_{fc,in} = 2.11 \times 10^{-4}$ m s^{-1}, (b) $\xi_a = 2$ or $v_{fc,in} = 4.21 \times 10^{-4}$ m s^{-1}, (c) $\xi_a = 3$ or $v_{fc,in} = 6.32 \times 10^{-4}$ m s^{-1}, and (d) $\xi_a = 4$ or $v_{fc,in} = 8.42 \times 10^{-4}$ m s^{-1}.

acid solution is taken high enough; which means that the amount of methanol crossover to the cathode side is negligible for all cases.

The effect of the fuel channel inlet velocity on the methanol concentration distribution for different stoichiometric flow coefficients, at the cell voltage of 0.4 V, is shown in Fig. 4a–d. It can be seen from these figures that, for any given flow rate, methanol concentration decreases along the thickness and flow directions. The main reasons for these decreases are the consumption of methanol at the ACL due to the electrochemical reaction and the drag of methanol through AM due to the electro-osmosis effect. The crossover methanol is almost completely washed away at the FEC due to the convective effect of the sulfuric acid solution pumped to the cell. The remaining little amount of methanol is spent during the chemical reaction occurring at the CCL. In this study, we assume that this reaction occurs at the interface CCL and CM; and the concentration of methanol becomes zero at this interface. Fig. 4a–d also shows that as the stoichiometric flow coefficient or the fuel channel inlet velocity increases, the concentration difference between the inlet and exit of the cell decreases. For example, the average methanol concentration at the exit of the fuel channel is 828 mol m^{-3}, 1353 mol m^{-3}, 1547 mol m^{-3}, and 1649 mol m^{-3} when the stoichiometric flow coefficient at the fuel channel inlet is taken as 1, 2, 3 and 4, respectively, for the given input data. These results show that more methanol is wasted (i.e. less methanol is utilized) when the fluid velocity at the fuel channel inlet increases.

The effect of the fluid velocity at the inlet of the fuel channel on the cell voltage and power density is shown in Fig. 5. As it can be seen from this figure, the trend of the polarization curves does not change significantly for different stoichiometric coefficients. However, the limiting current density increases as this coefficient increase; thus lower fuel channel inlet velocities cause a more limited operating range for the fuel cell. These trends are compared with the experimental study by Ge and Liu [21]; and it is seen that they are in good agreement with each other. In addition, this figure shows that higher maximum power densities could be achieved with higher stoichiometric coefficients. Numerically, the maximum power densities are found as 600 W m^{-2}, 670 W m^{-2}, 720 W m^{-2}, and 730 W m^{-2} when the stoichiometric flow coefficients at the fuel channel inlet are taken as 1, 2, 3 and 4, respectively. On the other hand, an increase in the flow rate of the methanol pumped to the fuel cell causes an increase in the power demand of the fuel pump; however this demand is not considered in this study as the

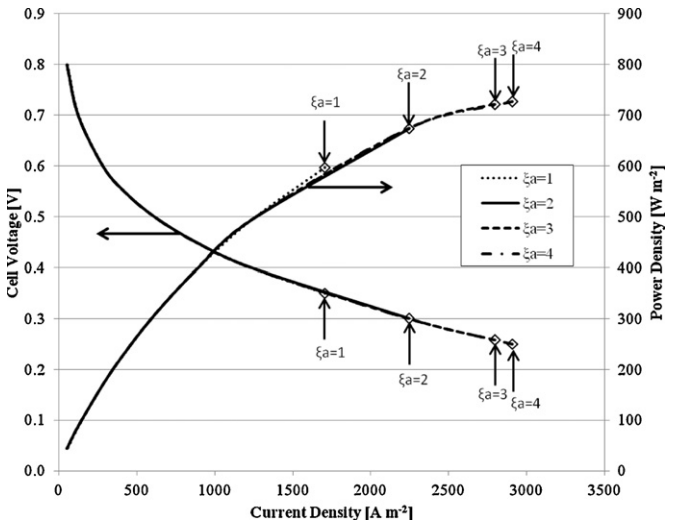

Fig. 5. Cell voltage and power density of the FE-DMFC for different fuel channel inlet velocities. (The limiting current densities are shown with arrows.)

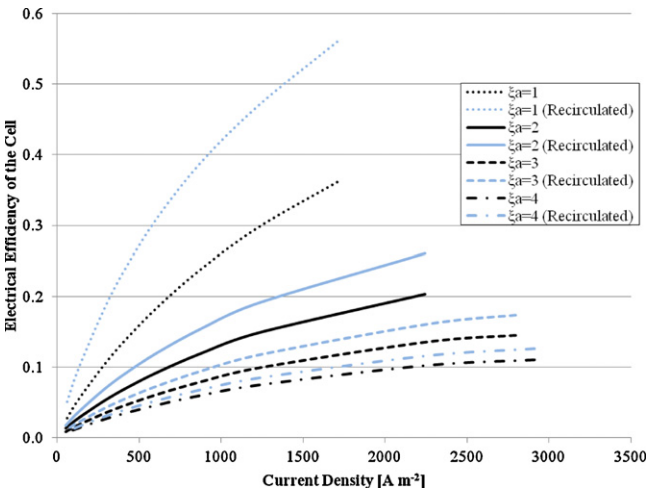

Fig. 6. Electrical efficiency of the FE-DMFC and recirculated FE-DMFC for different fuel channel inlet velocities.

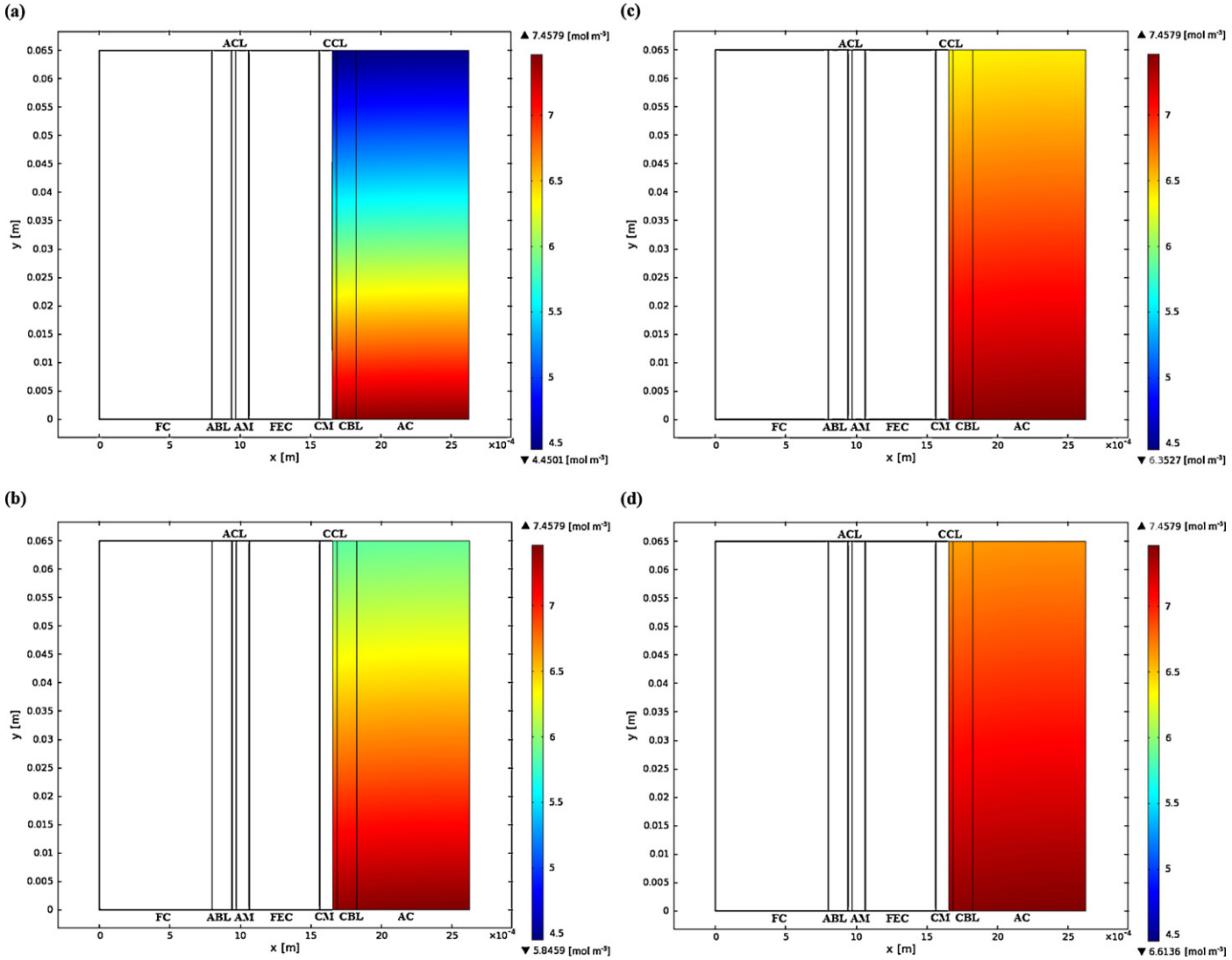

Fig. 7. Oxygen concentration distribution of the FE-DMFC for different air channel inlet velocities: (a) $\xi_c = 1$ or $v_{ac,in} = 8.47 \times 10^{-2}$ m s^{-1}, (b) $\xi_c = 2$ or $v_{ac,in} = 16.94 \times 10^{-2}$ m s^{-1}, (c) $\xi_c = 3$ or $v_{ac,in} = 25.41 \times 10^{-2}$ m s^{-1}, and (d) $\xi_c = 4$ or $v_{ac,in} = 33.88 \times 10^{-2}$ m s^{-1}.

focus of the study is the cell itself rather than the complete system including balance of plant.

The fluid velocity at the fuel channel inlet affects the electrical efficiency of the cell significantly, as can be seen in Fig. 6. The ratio of the total amount of the methanol utilized to the methanol entering the fuel cell increases as the fluid velocity decreases; which in turn leads to an increase in the electrical efficiency of the cell. Hence, lower stoichiometric coefficients at the fuel channel inlet are desirable to obtain higher electrical efficiencies. However, it should be kept in mind that lower maximum power densities are also achieved at these coefficients. Therefore, since power density and electrical efficiency cannot be maximized at the same time, the choice of the fluid velocity at the fuel channel inlet mainly depends on the purpose of the device and economical factors such as the fuel cost and the purchase and operation costs of the fuel cell. However, these considerations are out of the scope of the paper.

The electrical efficiency of the FE-DMFC can be further increased if the methanol leaving the FEC can be recovered, separated from sulfuric acid and recirculated back to the methanol storage tank. Kordesch et al. [7] proposed such a configuration including a separator to their basic design. As less amount of methanol enters the fuel cell at a given time due to the addition of this recirculation loop, the electrical efficiency of a recirculated FE-DMFC at a given stoichiometric coefficient becomes higher than that of a FE-DMFC, which can also be seen in Fig. 6. The maximum electrical efficiency that can be achieved for the recirculated FE-DMFC is found to be 56% when the stoichiometric coefficient is taken as 1 and the current density is equal to 1700 A m^{-2}.

3.3. Effect of the fluid velocity at the air channel inlet

The velocity of the air entering the fuel cell is another important parameter that can affect the performance of the system. This velocity can be represented by a stoichiometric flow coefficient as shown in Eq. (28). The value of this velocity depends on this coefficient, the geometry of the cell, oxygen concentration at the air channel inlet, and the reference current density, which is taken as 1500 A m^{-2}. In this paper, the effect of this coefficient on the oxygen concentration, cell voltage, power density, and electrical efficiency is studied. On the other hand, this coefficient has also an effect in preventing the cathode flooding and the power demand of the air blower; however these effects are not considered in this paper.

The oxygen consumption at the CCL due to the electrochemical reaction and the oxidation of the crossover methanol results in a decrease in the oxygen concentration at the flow direction, which can be seen in Fig. 7a–d. These figures also show the oxygen concentration distribution in a FE-DMFC for different stoichiometric flow coefficients when the cell voltage is 0.4 V. The concentration difference along the inlet and exit decreases as this coefficient increases. Numerically, for the oxygen concentration at the air channel inlet as 7.46 mol m^{-3}, this concentration at the air channel outlet is calculated as 4.45 mol m^{-3}, 5.85 mol m^{-3}, 6.35 mol m^{-3}, and 6.61 mol m^{-3} when the stoichiometric flow coefficients at the air channel inlet are taken as 1, 2, 3, and 4, respectively. These results show that more air is wasted (i.e. less air is utilized) for higher coefficients.

The effect of the air velocity entering the cell on the cell voltage and power density of the FE-DMFC is shown in Fig. 8. This figure shows that there is a slight increase in the performance of the cell as the velocity increases. The trend of this increase is in good agreement with the experimental data published by Ge and Liu [21]. This increase can be explained as follows: the cathodic current density is proportional to the concentration of oxygen at the CCL as shown in Eq. (14). This concentration increases with an increase in the air velocity; hence the cathodic overpotential decreases and the performance of the cell increases.

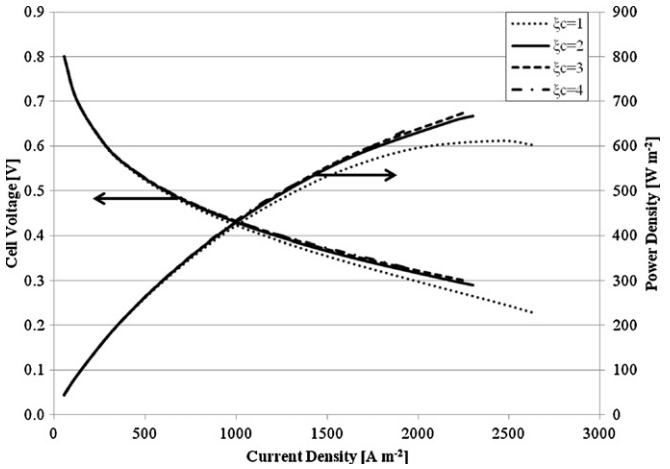

Fig. 8. Cell voltage and power density of the FE-DMFC for different air channel inlet velocities.

Fig. 9 shows the electrical efficiency of the cell for the FE-DMFC and recirculated FE-DMFC for different stoichiometric flow coefficients at the air channel inlet. This figure shows that as the air flow rate increases the electrical efficiency increases since there is no change in the fuel entering the system and power density increases. As discussed in Section 3.2, this efficiency can be further increased if a recirculation loop is used for the methanol leaving the FEC. For example, the electrical efficiencies of the recirculated FE-DMFC, for the cell voltage as 0.4 V and stoichiometric flow coefficient at the fuel channel inlet as 2, are found as 17.8%, 18.8%, 19.1%, and 19.2% when the stoichiometric flow coefficients at the air channel inlet are taken as 1, 2, 3, and 4, respectively. Here, it should be noted that the trend of the electrical efficiency of the system including balance of plant such as air blower could be slightly different as the power demand of the blower increases slightly. However, this demand is not considered in this study.

3.4. Effect of the fluid velocity at the flowing electrolyte channel inlet

The amount of methanol reaching the cathode side can be mainly controlled by adjusting the velocity of the sulfuric acid pumped through the FEC. Assuming a fully developed laminar flow condition, this velocity varies only with thickness direction and

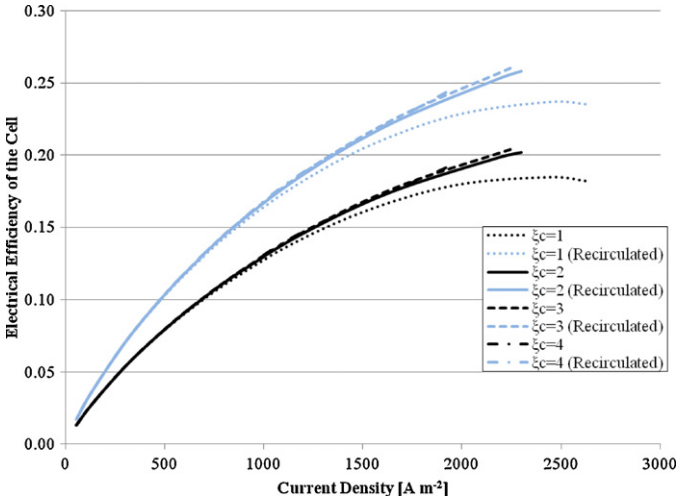

Fig. 9. Electrical efficiency of the FE-DMFC and recirculated FE-DMFC for different air channel inlet velocities.

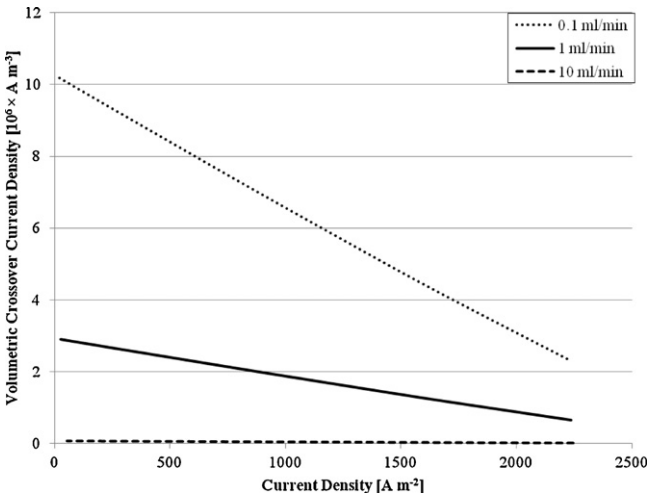

Fig. 10. Crossover current density of the FE-DMFC for different volumetric flow rate of flowing electrolyte.

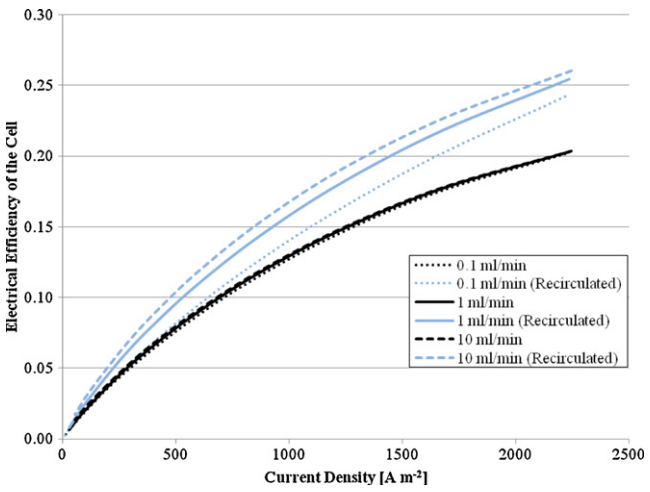

Fig. 12. Electrical efficiency of the FE-DMFC and recirculated FE-DMFC for different volumetric flow rate of flowing electrolyte.

depends on the volumetric flow rate of the sulfuric acid, number of repeat element, and the geometry of the cell, as shown in Eq. (26). Fig. 10 shows the change of the volumetric crossover current density, which is a measure of the amount of crossover methanol, with different volumetric flow rates of sulfuric acid: 0.1 ml min^{-1} (1.67×10^{-9} m^3 s^{-1}), 1 ml min^{-1} (1.67×10^{-8} m^3 s^{-1}), and 10 ml min^{-1} (1.67×10^{-7} m^3 s^{-1}). These flow rates correspond to the following average fluid velocities respectively: 5.21×10^{-5} m s^{-1}, 5.21×10^{-4} m s^{-1}, and 5.21×10^{-3} m s^{-1}. This figure shows that high flow rates such as 10 ml min^{-1} should be taken to eliminate the effect of the methanol crossover. This result is as expected since the convective flow at the flow direction gets more influential to sweep away the crossover methanol at the higher flow rates.

The effect of the volumetric flow rate of the sulfuric acid on the cell voltage and power density of the FE-DMFC is shown in Fig. 11. In a FE-DMFC, the addition of the FEC increases the ohmic losses; whereas it decreases the cathodic overpotential. When the thickness of the FEC is kept at its minimum value, the ohmic losses associated with this FEC could be minimized; and the flow rate of the FEC becomes the main operating parameter affecting the performance of the cell. Figs. 11 and 12 show that the performance of the cell slightly increases with an increase in the flow rate of the FEC. However, the electrical efficiency of the cell increases substantially if a recirculation loop is used, as shown in Fig. 12. For example, when the stoichiometric flow coefficients at the fuel and air channel inlets are taken as 2 and 3, the maximum electrical efficiency and power density that can be achieved are found as 26% and 670 W m^{-2}, respectively.

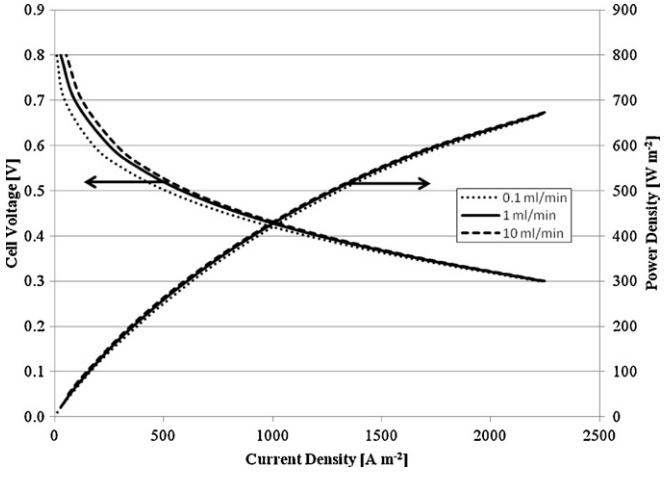

Fig. 11. Cell voltage and power density of the FE-DMFC for different volumetric flow rate of flowing electrolyte.

4. Conclusions

A two-dimensional multi-physics model has been developed to simulate the performance of the cell and to study the effects of some of the key operating parameters. These parameters include the fluid velocity at the fuel, air, and flowing electrolyte channel inlets. Using this model, the concentration distributions of the species, such as methanol and oxygen, along the thickness and flow directions, the cell voltage, the power density, and the electrical efficiency of the cell are found. The main findings of this study are listed below.

- There is a good agreement between the results of the model and the experimental data.
- As the stoichiometric flow coefficient at the fuel channel inlet increases (i.e. as the fluid velocity at the fuel channel inlet increases), higher power densities could be achieved; however less methanol is utilized and the electrical efficiency of the cell decreases.
- An increase in the stoichiometric flow coefficient at the air channel (i.e. an increase in the fluid velocity at the air channel inlet) yields to an increase in both the power density and the electrical efficiency of the cell.
- The electrical efficiency of the FE-DMFC can be further increased if the methanol leaving the FEC is recirculated to the methanol storage tank.
- The velocity at the FEC inlet should be taken high enough to eliminate the methanol crossover to the cathode side.

In this study, some operating parameters are suggested to increase the performance of a FE-DMFC. The results and main findings of the simulations conducted are expected to help in the development of the FE-DMFC to be used in portable applications. A 3D model will be developed as a future work to have a more accurate model and to find the distributions of the output parameters in all three directions.

Acknowledgement

Financial support for this work was provided by the Mitacs Elevate program and Ryerson University.

References

[1] C.O. Colpan, I. Dincer, F. Hamdullahpur, in: S. Kakac, A. Pramuanjaroenkij, L. Vasiliev (Eds.), Mini-Micro Fuel Cells: Fundamentals and Applications, NATO Science for Peace and Security Series, Springer, Netherlands, 2008, pp. 87–101.
[2] C.Y. Wang, in: S. Kakac, A. Pramuanjaroenkij, L. Vasiliev (Eds.), Mini-Micro Fuel Cells: Fundamentals and Applications, NATO Science for Peace and Security Series, Springer, Netherlands, 2008, pp. 235–242.
[3] K. Cowey, K.J. Green, G.O. Mepsted, R. Reeve, Current Opinion in Solid State & Materials Science 8 (2004) 367–371.
[4] V. Neburchilov, J. Martin, H. Wang, J. Zhang, Journal of Power Sources 169 (2007) 221–238.
[5] A. Serov, C. Kwak, Applied Catalysis B: Environmental 90 (2009) 313–320.
[6] S.K. Kamarudin, F. Achmad, W.R.W. Daud, International Journal of Hydrogen Energy 34 (2009) 6902–6916.
[7] K. Kordesch, V. Hacker, U. Bachhiesl, Journal of Power Sources 96 (2001) 200–203.
[8] J. Ge, H. Liu, Journal of Power Sources 160 (2006) 413–421.
[9] W. Liu, C.-Y. Wang, Journal of the Electrochemical Society 154 (3) (2007) B352–B361.
[10] W.W. Yang, T.S. Zhao, Electrochimica Acta 52 (2007) 6125–6140.
[11] J. Ge, H. Liu, Journal of Power Sources 163 (2007) 907–915.
[12] G. Murgia, L. Pisani, A.K. Shukla, K. Scott, Journal of the Electrochemical Society 150 (9) (2003) A1231–A1245.
[13] W. Liu, C.-Y. Wang, Journal of Power Sources 164 (2007) 189–195.
[14] F. Liu, G. Lu, C.-Y. Wang, Journal of the Electrochemical Society 153 (3) (2006) A543–A553.
[15] G.Q. Lu, F.Q. Liu, C.-Y. Wang, Electrochemical and Solid-State Letters 8 (1) (2005) A1–A4.
[16] E. Kjeang, J. Goldak, M.R. Golriz, J. Gu, D. James, K. Kordesch, Fuel Cells 4 (2005) 486–498.
[17] E. Kjeang, J. Goldak, M.R. Golriz, J. Gu, D. James, K. Kordesch, Journal of Power Sources 153 (2006) 89–99.
[18] C.O. Colpan, C.A. Cruickshank, E. Matida, F. Hamdullahpur, Journal of Power Sources 196 (2011) 3572–3582.
[19] D. Ouellette, C.O. Colpan, E. Matida, C.A. Cruickshank, Proceedings of the ASME 2011 9th Fuel Cell Science, Engineering and Technology Conference (FuelCell2011), August 7–10, 2011, Washington, DC, USA, 2011.
[20] C.Y. Wang, in: S. Kakac, A. Pramuanjaroenkij, L. Vasiliev (Eds.), Mini-Micro Fuel Cells: Fundamentals and Applications, NATO Science for Peace and Security Series, Springer, Netherlands, 2008, pp. 243–256.
[21] J. Ge, H. Liu, Journal of Power Sources 142 (2005) 56–69.
[22] DuPont Fuel Cells, http://www2.dupont.com/FuelCells/en_US/products/literature.html (accessed on 23.09.11).
[23] S.H. Jung, Modeling and control of two-phase flow in direct methanol fuel cells, A Dissertation in Mechanical Engineering, The Pennsylvania State University, 2010.
[24] K. Scott, W. Taama, J. Cruikshank, Journal of Power Sources 65 (1997) 159–171.
[25] V.B. Oliveira, D.S. Falcao, C.M. Rangel, A.M.F.R. Pinto, International Journal of Hydrogen Energy 33 (2008) 3818–3828.
[26] G. Lu, C.Y. Wang, in: B. Sunden, M. Faghri (Eds.), Transport Phenomena in Fuel Cells, WIT Press, 2005, pp. 317–350.
[27] H.E. Darling, Journal of Chemical and Engineering Data 9 (3) (1964) 421–426.
[28] W. Liu, C.-Y. Wang, Journal of Power Sources 164 (2007) 561–566.
[29] J.P. Meyers, J. Newman, Journal of the Electrochemical Society 149 (6) (2002) A718–A728.